Trends in analytical separations of magnetic (nano)particles

Mónica N. Alves[1], Manuel Miró[2], Michael C. Breadmore[1], Mirek Macka[1,3,4]*

1 School of Natural Sciences and Australian Centre for Research on Separation Science (ACROSS), University of Tasmania, Hobart 7001, Australia

2 FI-TRACE group, Department of Chemistry, University of the Balearic Islands, Carretera de Valldemossa, km. 7.5, E-07122 Palma de Mallorca, Spain

3 Department of Chemistry and Biochemistry, Mendel University in Brno, Zemedelska 1, 613 00 Brno, Czech Republic

4 Central European Institute of Technology, Brno University of Technology, Purkynova 123, 612 00 Brno, Czech Republic

*Corresponding author

Professor Mirek Macka, Private Bag 75, School of Natural Sciences and Australian Centre for Research on Separation Science, University of Tasmania, Hobart 7001, Australia

E-mail: Mirek.Macka@utas.edu.au

Phone: +61 362266670; Fax: +61 362262858

Keywords:

Capillary electrophoresis; field flow fractionation; magnetic (nano)particles; magnetophoresis; microfluidic chip; separation

Abstract

Magnetic particles (MPs) and magnetic nanoparticles (MNPs) are appealing candidates for biomedical and analytical applications due to their unique physical and chemical properties. Given that magnetic fields can be readily used to control the motion and properties of M(N)Ps, their integration in analytical methods opens new avenues for sensing and quantitative analysis. There is a large body of literature related to their synthesis, with a relatively small number of methods reporting the analysis of M(N)Ps using separation methods, which provide information on their purity and monodispersity. This review discusses analytical separation methods of M(N)Ps published between 2013 and June 2018. The analytical separation methods evaluated in this work include (i) field flow fractionation, (ii) capillary electrophoresis, (iii) macroscale magnetophoresis and (iv) microchip magnetophoresis. Among the trends in analytical separations of M(N)Ps an inclination towards miniaturization is moving from conventional benchtop methods to rapid and low-cost methods based on microfluidic devices.

Contents

1 Introduction

Magnetic (nano)particles (M(N)Ps) offer the unique advantage of being manipulated (moved or held in place) using permanent magnets or electromagnets, a significant reason behind their popularity, which grew rapidly in the past decades [1-3]. As an example, one of the most routinely used methods exploiting MPs is magnetic sorting of cell populations from biological suspensions [4]. This method is now standardized for tissue engineering and medical analysis.

Magnetic nanoparticles (MNPs) exhibit physical properties that differ remarkably from those of the bulk ferromagnetic material due to finite size effects such as high surface-to-volume ratio, and a special magnetic property at diameters typically lower than 20 nm called superparamagnetism [5]. At such small size, MNPs do not exhibit multiple magnetic domains like ferromagnetic particles, but instead a single domain. Therefore, under an external magnetic field, the magnetic moment of single domain nanoparticles quickly aligns with the applied field, but in its absence, they exhibit no net magnetisation due to the rapid reversal of their magnetic moment. It makes superparamagnetic nanoparticles especially suitable when looking for fast responses to external magnetic fields without agglomeration effects [6]. For this reason, superparamagnetic nanoparticles have been extensively pursued for a vast variety of biomedical applications, including biosensing [7], bioanalysis [8], drug delivery [9], magnetic resonance imaging (MRI) [10], and hyperthermia treatment of tumours [11].

The unique behavior and increasing applications of M(N)Ps have stimulated the advancement of new synthesis methods. The core of M(N)Ps can be made of a wide range of magnetic materials such as nickel, cobalt, iron and iron oxides. Iron oxides and their corresponding ferrites are the most commonly used due to their high magnetic moments, biological compatibility, simple synthesis and low cost of production. However, bare iron oxide nanoparticles are only stable in low ionic strength solutions at pH values above (pH 9 - 12) or below (pH 2 - 5) their point zero charge. To prevent aggregation and increase selectivity, the magnetic cores are usually coated with inorganic materials [12], polymers [13-16] and/or functionalised with organic and biological molecules [1, 17]. There is a large quantity of literature exploiting

the synthesis and surface engineering of M(N)Ps for many purposes. Compared to this large output, the body of reports on separation approaches used for the analysis of M(N)Ps is considerably smaller, but still very significant. A search in Elsevier's database Scopus shows that only ca. 12% of the total publications on M(N)Ps address analytical separation techniques. Yet, the separation and analysis of M(N)Ps is critically important to obtain information on their size, shape and chemistry surface, enabling their practical use for many applications.

In 2012, Stephens *et al*. [18] reviewed 58 papers describing separation of M(N)Ps by means of applied magnetic fields and field gradients for improved purification and analysis [18]. The main goal of this review is to pinpoint separation techniques of M(N)Ps for the period between 2013 and June 2018, by employing three distinct types of field-flow fractionation (FFF) (magnetic FFF, asymmetrical FFF and cyclical electrical FFF), capillary electrophoresis (CE), macroscale magnetophoresis (high/low gradient magnetic separation), and microchip magnetophoresis. Analytical separation and sample preparation approaches using M(N)Ps are deemed outside the scope of our review, for which there is a large body of literature, including recent comprehensive reviews [1-3, 19-23]. All the studies discussed and critically analyzed are summarized in table 1 in terms of particle composition and size, magnetic field applied, separation principle, separation time and complexity of the infrastructures used.

2 Separations of magnetic (nano)particles

2.1 Field flow fractionation

FFF is a separation technique that uses an external field applied perpendicular to the direction of flow causing differential migration of M(N)Ps. Typically, the flow profile in a FFF channel is laminar, so particles which interact more strongly with the field are found closer to the channel walls and will move more slowly due to slower flow streams. Analytes can be separated by different mechanisms of FFF according to the type of the field applied. Typical fields include centrifugal and gravitational forces, cross flow of solvent, and thermal, electrical and magnetic gradients [24].

2.1.1 Magnetic field flow fractionation

Magnetic field flow fractionation (MFFF) has been shown to be an effective method for the separation of polydisperse suspensions of M(N)Ps when an external magnetic field is applied along a flowing channel. Rogers *et al.* [25] used MATLAB to simulate the separation of fluidMAG-D (starch-coated magnetite (Fe_3O_4)) M(N)Ps of sizes between 50 and 400 nm by simulating particle trajectories and magnetic forces. The results obtained from the simulation showed that M(N)Ps within the size range of interest could be separated and collected in a size dependent manner in fraction 1 (smaller sized) and fraction 2 (larger sized). To validate this model, the simulated conditions were replicated experimentally. However, the theoretical and experimental results did not agree. This inconsistency could be due to the fact that particle-particle interactions are not taken into consideration into the model. Due to the failure of the initial experiments, the same authors changed the approach to a simple magnetic coil setup composed of a tubing wrapped around a Grade N42 diametrically magnetized neodymium cylinder [25]. An inlet for both the M(N)Ps suspension and the mobile phase was inserted at the top of the magnetic coil and a single outlet at the bottom was used for the collection of magnetic particle fractions. The tubing was filled with M(N)Ps suspension. As soon as a steady state level of accumulation of M(N)Ps across the inner wall of the tubing was achieved, an initial flow rate of 0.25 mL/min was applied to wash out the M(N)Ps remaining suspended. Then, the flow rate was increased up to 50 mL/min. DLS measurements and TEM showed that the particles collected at lower flow rates were smaller than particles collected at higher flow rates. This approach was low cost and allowed the separation of polydisperse M(N)Ps by simply controlling the flow rate. However, broad size distributions were obtained. Thus, further optimisation of the system is crucial to allow for specific applications such as in biomedicine.

2.1.1.1 Magnetic quadrupole field flow fractionation

The first prototype of a magnetic quadrupole field flow fractionation (MQFFF) was developed and evaluated by Zborowski *et al*. [26] for continuous separation of human peripherical lymphocytes labeled with magnetic colloids. It consisted of a quadrupole electromagnet assembly of four steel pole tips with two

of them opposed the magnetic north poles and the other two opposed the magnetic south poles. The electromagnet assembly was radially symmetric. The steel was magnetized by an electric current in the coils wrapped around the poles. This configuration creates a magnetic field whose magnitude increases linearly with the radial distance from the axis. This methodology is well described by Carpino *et al.* [27]. The results showed that the separation process was close to the predicted behavior of an ideal quadrupole magnetic field [26]. Later on, Orita *et al.* [28] developed a simple on-off field MQFFF to separate and quantify two distinct sub micrometer commercial M(N)Ps (90 and 200 nm) at specific magnetic field and flow conditions [28]. This on-off field MQFFF system was inspired by the system previously developed by Zborowski *et al*. [26] . It consisted of a separation channel volume of 0.94 mL fitted into a stainless-steel cylinder that was implemented in a flow injection setup with downstream optical detection (Figure 1). The fractograms exhibited improved retention (98.6% vs. 53.3%) for the larger M(N)Ps (200 nm vs.90 nm) at higher flow rates (0.05 mL/min vs. 0.01 mL/min) [28]. Thus, for given field and flow conditions, the on-off field MQFFF system can be used for the quantification of retained and unretained fractions. This is useful for the separation of unwanted weakly magnetic particulate contaminants from M(N)P suspensions. Compared to the magnetic coil setup previously described, the on-off field MQFFF system requires less handling.

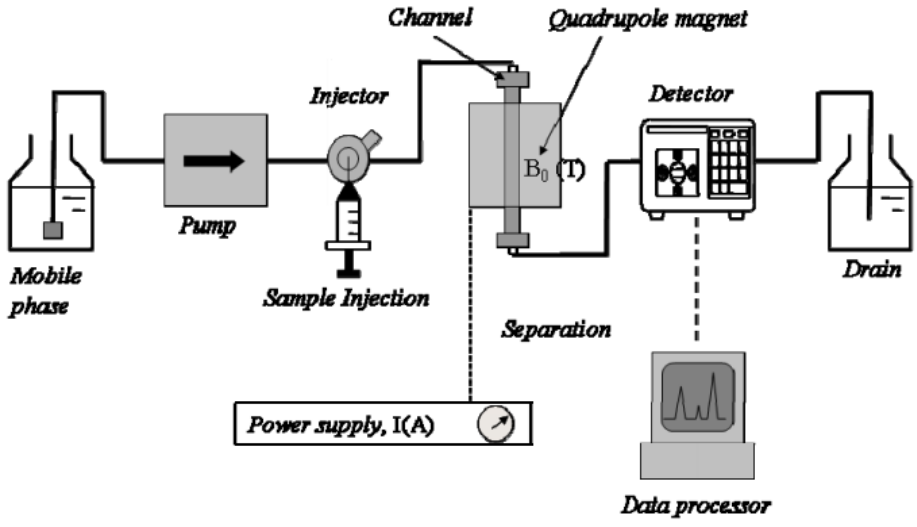

Figure 1 – Schematic of the MQFFF system. The mobile phase was driven by a pump. The sample is introduced through a separate port. The flow of the mobile phase pushes the sample from the injector into

149 the separation channel fitted into a quadrupole electromagnet connected to a UV-visible detector.
150 Reprinted from [28] with permission.
151
152 Moore *et al.* [29] used MQFFF for red blood cell (RBC, with mean diameter of 8 µm) separation as
153 an alternative to centrifugal separation. A quadrupole field was designed having a maximum field of 1.68 T
154 at the magnet pole tips, zero field at the aperture axis, and a nearly constant radial field gradient of 1.75 T
155 mm^{-1} inside a cylindrical aperture. A light-scattering detector downstream of the magnet measured light
156 attenuation caused by the cells eluting from the magnet as a function of time. The cell samples were
157 composed of high spin RBC (obtained by chemical conversion of hemoglobin to methemoglobin - met RBC
158 - or exposure to anoxic conditions - deoxy RBC), low spin RBC (obtained by exposure to ambient air – oxy
159 RBC), and mixtures of deoxy RBC and white blood cells (WBC). Cell tracking velocimetry was used to
160 measure the magnetophoretic mobility of the RBC and the results showed that the mobility depended on
161 the presence of high-spin hemoglobin. Only high spin RBC were attracted by the magnet, while low-spin
162 RBC demonstrated magnetic susceptibility comparable to WBC. It was also found that RBC did not elute
163 within 15 min from the channel at flow rate ≤ 0.05 mL/min but as would be expected rapidly eluted at a
164 higher flow rate of 2.0 mL/min. These results agreed with earlier studies on the magnetic properties of
165 hemoglobin using other techniques [30, 31]. The fractionation experiments of RBC and a RBC/WBC mixture
166 showed that a 5 x 10^7/mL cell suspension pumped at 0.1 mL/min through a magnetic field of 1.5T and
167 gradient of 1,000 T m^{-1} is depleted to less than 5% of the initial RBC number concentration. The 5% residual
168 contamination was comparable to that typically seen in WBC obtained by blood centrifugation. One
169 advantage over blood centrifugation, is that MQFFF RBC separation can be scaled to microliter devices for
170 RBC debulking, which can be portable and operated immediately after donation with minimal human labor.
171

172 2.1.2 Asymmetrical flow field-flow fractionation

173 Asymmetrical flow field flow fractionation (AF4) is a separation technique based on the theory of
174 FFF. The cross flow is induced by flowing liquid constantly exiting through a semi-permeable wall on the

bottom of the channel. The lower size M(N)Ps, which can be fractioned, are restricted by the molecular weight cut off membrane. The suitability of AF4 has been shown for the fractionation of magneto polyplexes (with mean diameter of 54 nm) [32] and carboxydextran-coated maghemite dispersions (with diameter of 6 – 60 nm) [33] by connecting the AF4 instrument to UV [33] and multi-angle laser light scattering (MALLS) [32, 33] detectors. AF4 can be a simple, fast and reliable tool for quality control in commercial production of M(N)Ps, while providing complementary information related to nonmagnetic sample components.

2.1.3 Cyclical electrical field flow fractionation

Cyclical electrical field flow fractionation (CyEFFF) consists of an oscillating square voltage applied between a top and bottom electrode inside the channel. As result, M(N)Ps move back and forth between the electrodes in agreement with their sizes and electrophoretic mobilities. M(N)Ps with high electrophoretic mobilities move further into the center of the channel and they spend more time at the faster fluid regions thus eluting earlier than the lower mobility M(N)Ps. One of the limitations of this technique is the band broadening of the resulting UV fractograms and low resolution. To address and solve the diffusion issue, Tasci *et al.* [34] reported the separation of MNPs by CyEFFF applying square wave voltages with higher duty cycles instead of DC offset voltages (Figure 2). Thus, particle diffusion was suppressed, which allowed separations of MNPs with mean diameter of 50 and 100 nm. This study demonstrated the capability of CyEFFF for size and electrophoretic analysis of lipid and polystyrene sulfonate-coated MNPs [34].

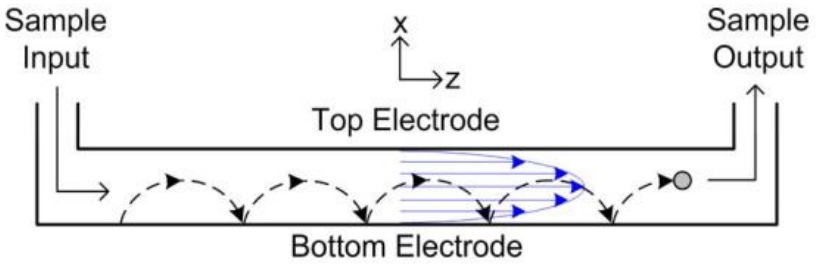

Figure 2 – Schematic of the CyEFFF system. The dashed line shows the particle trajectory that results from the cyclical electrical field. Reprinted from [34] with permission.

2.2 Capillary electrophoresis

CE is a powerful separation method which has the advantages of minimal requirement of sample and buffer volumes, and lack of generation of organic waste. Further, the use of narrow capillaries in CE with high electrical resistance, allows the application of high electrical fields with minimal heat generation. The use of high electrical fields together with the conventional plug-type flow from electrically driven systems results in short analysis times and high efficiency and resolution for almost any type of ionic analytes. Yet, a remarkable limitation of bare iron oxide M(N)P separations by CE that has been previously reported [35-38] is their high tendency to spontaneously agglomerate to minimize surface energies, which is observed in electropherograms as spurious spikes that in turn prevent the accurate determination of the electrophoretic mobilities of M(N)Ps. This limitation has been recently overcome by Alves *et al.* [39], who achieved symmetrical and smooth peaks of bare iron oxide nanoparticles. This was accomplished through electrostatic stabilisation using complexing electrolyte anions such as citrate and phosphate, and the additive tetramethylammonium hydroxide (TMAOH) within the background electrolyte (BGE), an ionic solution of desired concentration, co-ion and counter-ion mobilities, and usually also providing pH-buffering capacity. TMAOH is a peptizing agent (an electrolyte that converts aggregated particles into a colloidal sol) [40] used for more than two decades in the synthesis of well-dispersed iron oxide M(N)P solutions, however never utilised for effective CE separations of M(N)Ps. The same study also showed the successful separation of bare (with diameter between 7 and 13 nm) and carboxylated (10 nm) iron oxide nanoparticles in 12 min using Tris-nitrate containing 20 mM TMAOH as BGE. The electrophoretic mobilities for bare and carboxylated iron oxide nanoparticles were 3.3E-08 $m^2 V^{-1} s^{-1}$ (0.9 %RSD) and 4.1E-08 $m^2 V^{-1} s^{-1}$ (0.4 %RSD), respectively. These findings demonstrate that simple and rapid CE experiments are excellent tools to characterise and monitor properties and interactions of iron oxide nanoparticles with other molecules for potential surface modification purposes [39]. Baron *et al*. [41] studied the online stacking of carboxylated core-shell magnetite nanoparticles in CE. By monitoring the ionic strength of the BGE and the sample zone, it was observed that stacking occurred optimally when MNPs were dispersed in 10 mM borate/NaOH (pH 9.5) and injected to the BGE composed of 100 mM borate/NaOH (pH 9.5). The decrease of the electric

double layer thickness with increasing ionic strength could induce MNP aggregation and led to the restructuring of the MNPs zone due to the decrease of distance between nanoparticles [41]. The Derjaguin-Landau-Verwey-Overbeek (DLVO) theory, which describes van-der-Waals and electrostatic interactions between charged surfaces within a liquid medium [42], was suggested as a cause of peak sharpening in CE.

2.3 Macroscale magnetophoresis

Magnetophoresis refers to the motion of magnetic particles or magnetizable material through a fluid under the influence of a magnetic field [43]. For almost all the M(N)Ps applications, manipulation, recovery, and collection rates using external magnets should be done quickly. Rapid magnetophoretic separation can be attained under both high gradient (HGMS, $\nabla B^{\rightarrow} > 1000$ T m^{-1}) and low gradient magnetic separation (LGMS, $\nabla B^{\rightarrow} < 100$ T m^{-1}).

2.3.1 High gradient magnetic separation

HGMS is commonly employed in conventional industry practice to separate magnetic materials from non-magnetic aqueous solutions, such as for wastewater treatment of bacteria and solids. Typically, HGMS is used to separate microscale or bigger particles, or microscale aggregates of nanoparticles, or nanoparticles encapsulated in larger polymer beads. However, the application of HGMS to suspensions of individually dispersed M(N)Ps has been poorly explored so far. HGMS systems generally consist of a column packed with magnetically susceptible wires placed inside an electromagnet. Through application of a magnetic field across the column, the wires dehomogenise the magnetic field in the column producing high field gradients around the wires to enable the capture of M(N)Ps onto their surfaces. The attraction of M(N)Ps depends on the magnetic field gradients generated, particle size and magnetic properties [44]. A study conducted by Mirshahghassemi *et al.* [45] describes the application of HGMS for oil remediation using polyvinylpyrrolidone (PVP)-coated MPs (mean size diameter of 127 nm) in a continuous and large volume flow system. This technique was analyzed as a function of magnetic field strength, mixing time and stainless-

steel wool content. Fluorescence and inductively coupled plasma-optical emission spectrometer (ICP-OES) data indicated that ca. 85% of oil and 95% of MNP were eliminated. The continuous use of this HGMS system over 7 hours allowed the treatment of 17 liter oil water mixture with no reduction of the oil and MPs removal capacity [45]. Although this study introduces a new application of HGMS for oil remediation, it has the disadvantages of being tedious and time-consuming.

2.3.2 Low gradient magnetic separation

In contrast to conventional practice where HGMS is normally employed, LGMS is still poorly explored and understood. Toh *et al.* [46, 47] showed the reliability of LGMS for magnetophoretic separation of microalgal biomass that interacted electrostatically with cationic polymer functionalized MNPs [46, 47]. Poly (diallyl dimethylammonium chloride) (PDDA) and chitosan (Chi) (with mean diameter of 50 nm) worked as binding agents to promote rapid separation of the negatively charged *Chlorella* sp. through LGMS at field gradient lower than 80 T m^{-1}. The obtained results indicated cell separation efficiency of about 98% for PDDA and 99% for Chi. Though, from a practical point of view, PDDA was preferable as polymer binder since the attachment mechanism involved was pH independent [47]. Because almost all the magnetophoretic studies have been dedicated to the behavior of spherical MNPs, and poor attention has been paid to rod-like MNPs, Lim *et al.* [48] compared the magnetophoretic behavior of spherical and rod-like iron oxide nanoparticles under LGMS. Both effects of particle concentration and magnetic field gradient on the separation kinetics were evaluated. It was shown that at low particle concentration, the magnetophoresis of MNPs at low magnetic gradient is significantly enhanced by particle anisotropy (non-spherical shape), with rod-like MNPs taking significantly less time than spherical MNPs to be separated [48]. New approaches for the separation of M(N)Ps according to their shape, size, and coatings, along with their unique magnetic properties will open new opportunities for M(N)Ps.

2.4 Microchip magnetophoresis

The field of microfluidics is continuously evolving as miniaturized platforms provide quick analysis with high resolution at low cost, foster portability and make use of exceptionally minute amounts of reagents. Zhang *et al*. [49] developed a microchip based on magnetophoresis with differential interference contrast (DIC) detection (Figure 3A and 3B). The real-time moving trajectories and velocities of the MPs at different magnetic field strengths (depending on the distance to the permanent magnet) were measured based on consecutive DIC images. The results indicated that shorter distances to the magnet caused higher magnetophoretic velocities of MPs, and enhanced magnetophoretic velocity differences between dissimilar particle sizes (Figure 3D) [49]. This study allowed the successful separation and detection of a polydisperse mixture of MPs (500 nm and 160 nm) at a single-particle level in only about 15 seconds (Figure 3C).

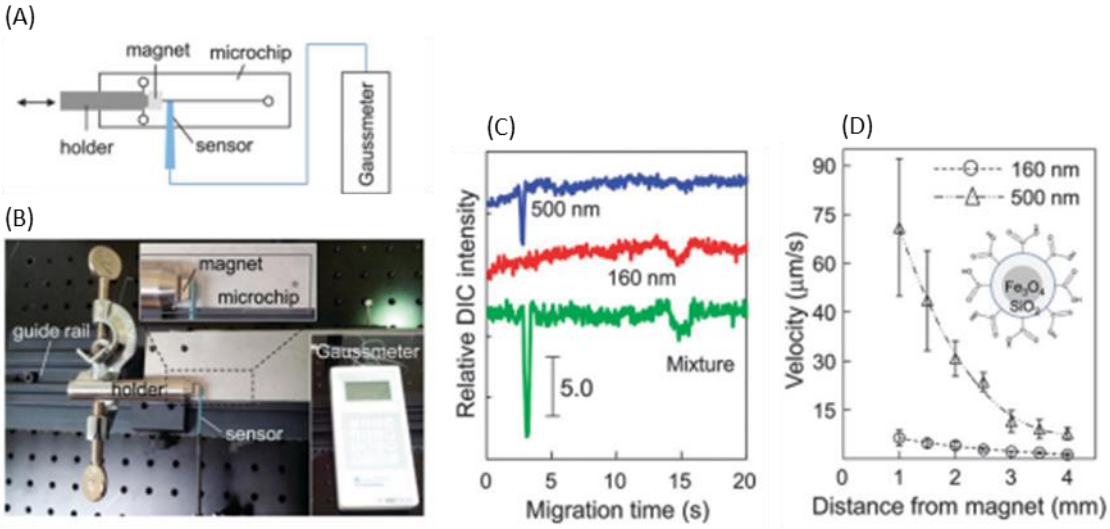

Figure 3 - Schematic diagram (A) and photography (B) of the experimental setup of the microchip magnetophoresis. (C) Representative magnetopherograms of the MPs by microchip magnetophoresis with the DIC detection system. (D) Magnetophoretic velocities of the MPs at different permanent magnet distances obtained using a DIC microscope. Reprinted from [49] with permission.

The microfluidic separation of iron oxide beads (5 µm diameter) with soft magnetic microstructures was demonstrated by Zhou *et al*. [50]. The fabrication process of the microfluidic device is represented in Figure 4. This microfluidic device consisted of two channels - fluidic and structural – made in polydimethylsiloxane (PDMS). The fluidic channel contained two inlets and two outlets. A mixture of iron

powder and PDMS was injected into the structural channel located between two external permanent magnets. Three microstructure shapes were studied: (i) half circle, (ii) 60° isosceles triangle and (iii) 120 ° isosceles triangle. The soft magnetic microstructures provided localized and strong magnetic forces on the MPs that deflected them perpendicularly to the pressure-driven flow. Thus, the separation depended on the magnetic forces. In turn, magnetic forces are affected by the shape of the iron-PDMS microstructures and the mass ratio of the iron-PDMS composite. Also, the flow rate in the fluid channel affects the time that MPs are subjected to the magnetic field, and consequently their vertical deflection. Numerical simulations were developed to predict the particle trajectories showing good agreement with experimental data. Finally, systematic experiments and simulations were conducted to study the effect of several relevant factors on the separation of MPs: microstructure shape, mass ratio of the iron–PDMS, microfluidic channel width and average flow velocity. The results demonstrated that (i) half circular iron–PDMS microstructure caused greater deflections, (ii) larger mass ratio of the iron–PDMS composite provided higher magnetic forces, and (iii) wider channels separate MPs less efficiently than narrow microfluidic channels when operating at the same flow rate [50]. Based on the obtained results, enhanced separations of MPs can be achieved in a compact, simple and low-cost microfluidic device.

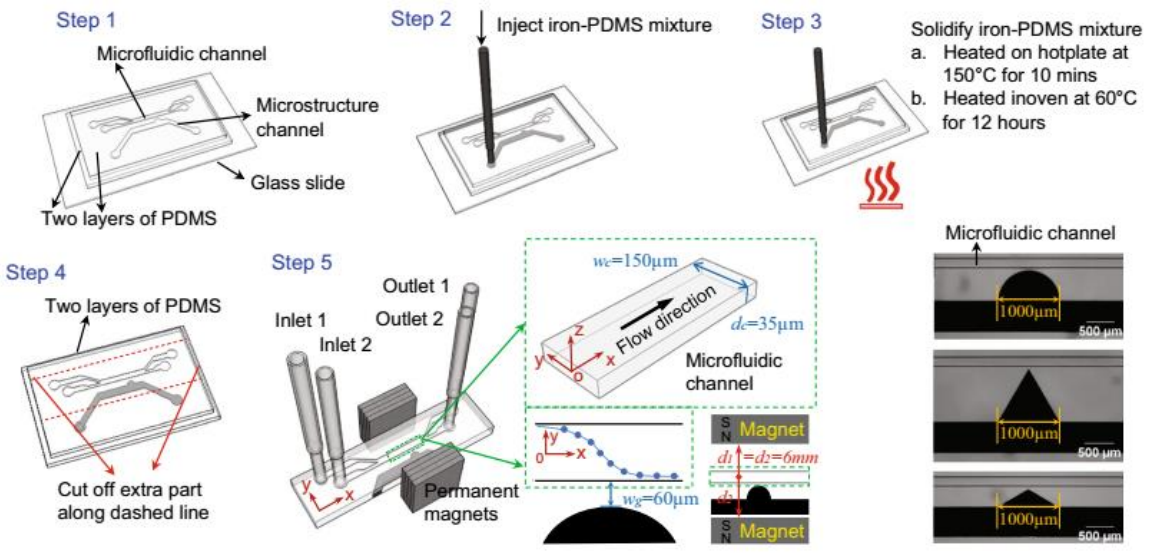

Figure 4 - Fabrication process of the microfluidic device for efficient separation of magnetic particles based on deflection in flowing streams. Reprinted from[50] with permission.

Kumar and Rezai [51] introduced a novel hybrid technique called multiplex inertio-magnetic fractionation (MIMF) to simultaneously fractionate up to four magnetic and non-magnetic particles in water at a throughput of $10^6 – 10^9$ particles per hour. The MIMF device was based on interactions between flow-induced inertial forces and magnetic forces in an expansion microchannel containing an external permanent magnet (Figure 5). The particle fractionation performance was first optimized in terms of flow rate and aspect ratio of the channel and particle size on duplex MIMF to understand the behavior of the particles. The obtained knowledge was then applied to demonstrate fourplex MIMF with three magnetic monodisperse particles (5, 11 and 35 μm) and nonmagnetic particles (15 μm). The non-magnetic particles inertially focus at the center of the channel, while magnetic particles get fractionated based on interaction between inertial and magnetic forces and positioned in a size related manner in the device with smaller particles located closer to the external magnet. The exit position for each particle type and size was measured with respect to the expansion region baseline since the focus of this study was only to investigate the concept of MIMF and not M(N)Ps sorting. In the future, outlets can be implemented based on the exit positions calculated. This MIMF device addresses several disadvantages of currently available magnetic fractionation devices such as low throughput, requirement of sheath flow and inability to fractionate multiple targets simultaneously [51].

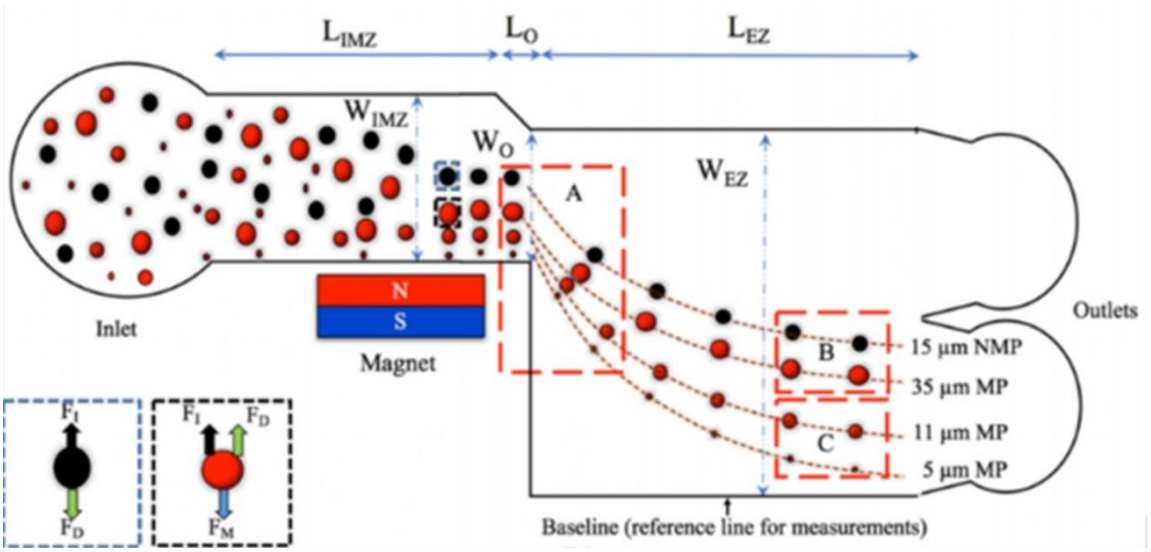

328

329 Figure 5 – MIMF scheme of the particle separation. The device (scale bar 25 mm) consisted of an inertio-
330 magnetic zone (IMZ) with a side permanent magnet and an expansion zone (EZ). The schematic
331 representation of MIMF device shows three red-colored magnetic particles (MP) of varied sizes and a black-
332 colored non-magnetic particle (NMP). Reprinted from [51] with permission.

333

334 Dutz *et al*. [52] studied the consequences of applying an external magnetic force to a suspension
335 of MPs with diameters of 2, 6 and 12 µm circulating in a spiral microfluidic channel (Figure 6). The fluid was
336 injected via an input port located near the center of the spiral and exits through a symmetric flow splitter
337 and two outlet ports. The exit ports were referred to as inner outlet and outer outlet, which collected the
338 inner and outer halves of the fluid stream, respectively. For that purpose, an array of permanent magnets
339 was arranged and accurately centered beneath the spiral to produce a magnetic field with octupolar
340 symmetry. At low flow rates (5 µL/min) it was observed that 6 µm MPs clustered along a streamline near
341 the outer wall of the spiral. At intermediate flow rates (30 µL/min), 6 µm MPs were homogeneously
342 distributed across the width of the channel. At high flow rates (60 µL/min), 6 µm MPs were focused in
343 clusters within the inner half of the spiral. The phenomenon observed at high flow rates was caused by
344 hydrodynamic drag forces that induced secondary (Dean) flow in the spiral microfluidic channel. A model

incorporating key forces involved in the spiral microchip was described and used to extract quantitative *in situ* information about the magnitude of local Dean drag forces from experimental data. The experimental results also showed that at low flow rates (5 µL/min) all the 12 µm MPs and one third of the 2 µm MPs were drawn toward the outer wall of the spiral and extracted from the outer outlet, whereas the remaining two thirds of the 2 µm MPs were extracted from the inner outlet. Gradually more 6 and 12 µm MPs were extracted from the inner outlet at higher flow rates. For example, all the 12 µm MPs were found to exit the inner outlet at 40 µL/min. The behavior of the smallest MPs (2 µm) was opposite of the larger particles, with less and less being extracted from the inner outlet as the flow rate increases. [52].

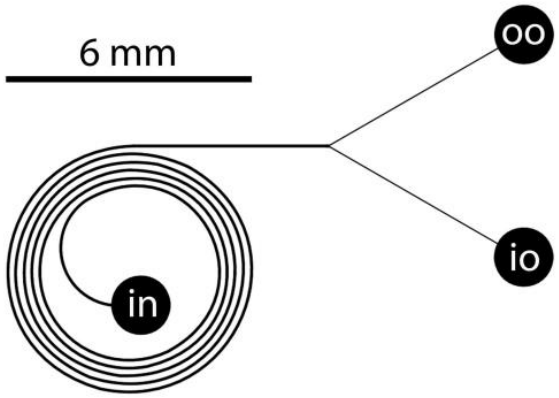

Figure 6 – Geometry of the microfluidic spiral. The fluid was injected via the input port (in) and exits through the exit ports referred as inner outlet (io) and outer outlet (oo). Reprinted from [52] with permission.

The effective application of MNPs is highly dependent of appropriate cleaning after synthesis and/or before their use to remove solvents, excess of surfactants, byproducts and undesired impurities. Because manual cleaning is time consuming and inefficient, Cardoso *et al*. [53] designed, fabricated and tested a microfluidic system for the continuous cleaning and separation of MNPs (average diameter of 10 nm) synthesized by coprecipitation using NH_4OH as catalyst. First, a theoretical study was performed to optimize the geometrical configuration of the microfluidic device and the experimental conditions. The optimized microfluidic system was composed of two inlets and two outlets (Figure 7). The cleaning solution (water, fluid A) was introduced through the inlet A and the synthesis solution with MNP (fluid B) through the inlet B. The waste fluid (fluid C) exited through the outlet C, whereas the cleaned MNPs solution (fluid

D) exited though the outlet D. A permanent magnet was located near the diffusion channel to deflect the MNPs by magnetic forces from the synthesis solution to the cleaning solution (figure 7). Gas chromatography was performed to indirectly calculate the cleaning efficiency by measuring the decrease of the peak area of NH_4OH. The results demonstrated a cleaning efficiency of about 99.7% by controlling the fluid flows in the microfluidic system, whereas manual cleaning achieved a value of about 94.3% after cleaning six consecutive times. Both processes are time-consuming, however the microfluidic system offers negligible loss of MNPs and the process is performed autonomously [53].

Figure 7 – Schematic of the optimized microfluidic system. Fluid A: cleaning solution; Fluid B: synthesis solution with MNPs; Fluid C: waste; Fluid D: cleaned MNPs. Channel widths (a) 600 µm; (b) 400 µm; (c) 600 µm; (d) 400 µm; diffusion channel length (e) 10 mm. Reprinted from [53] with permission.

The separation of magnetic particles with spherical (mean diameter of 7 µm) and elliptical shapes was demonstrated by Zhou *et al*. [54] in a simple and effective manner. The microfluidic chip consisted of two inlets and one outlet. The inlet 1 was injected with aqueous-glycerol solution that worked as buffer flow, while the inlet 2 was injected with sample particles suspended in aqueous-glycerol solution. The microfluidic device was placed in the center of a uniform magnetic field and mounted on an inverted microscope to record the trajectories of the magnetic particles. A pressure-driven flow was combined with the magnetic field applied perpendicularly to the flow direction. The results showed that the asymmetrical rotation of the ellipsoidal MPs, together with the particle-wall hydrodynamic interactions, resulted in a net

lift force towards the channel center. Differently, spherical MPs remained closer to the channel wall. This uniform magnetic field technique can be applied to multiple microfluidic channels facilitating high throughput parallelization for biological and biomedical applications that require separation of shaped MPs [54].

Conclusion and outlook

The improvement of the existing approaches of synthetizing uniform and more monodisperse M(N)Ps has been notorious in recent years. However, even the most efficient and highly optimized protocols yield samples relatively polydisperse. This is an obstacle for some emerging applications of M(N)Ps with some specific functions, particularly in biomedical areas, as their properties are dependent. Analytical tools for M(N)Ps separation are fundamental to understand the behavior of M(N)Ps according to their size, shape and surface chemistry. This knowledge can give information on the monodispersity and purity of M(N)Ps for their ultimate practical use. Over the last 5 years, novel strategies for M(N)P separations have been reported based on FFF, macroscale magnetophoresis and CE, but the trend is toward integrating external magnetic fields onto single microfluidic structures. From about 33 journal articles that have been published in the last 5 years, 54% of them are microfluidic based. These can be easily fabricated and are inexpensive, not requiring any extra power source. Moreover, separations in microchip magnetophoresis can be easily achieved with high efficiency and throughput in the order of seconds. Real-time moving trajectories and velocities of M(N)Ps can also be monitored by means of microscope imaging that is seen as the new trend in microfluidic separation and identification of M(N)Ps.

Acknowledgements

Mirek Macka gratefully acknowledges the Australian Research Council Future Fellowship (FT120100559). Manuel Miró acknowledges financial support from the Spanish State Research Agency (AEI) through project CTM2017-84763-C3-3-R (MINECO/AEI/FEDER, EU). Michael Breadmore acknowledges an Australian Research Council Future Fellowship Award (FT130100101).

References

[1] Á. Ríos, M. Zougagh, Recent advances in magnetic nanomaterials for improving analytical processes, TrAC, Trends Anal. Chem. 84 (2016) 72-83.

[2] T. Jamshaid, E.T.T. Neto, M.M. Eissa, N. Zine, M.H. Kunita, A.E. El-Salhi, A. Elaissari, Magnetic particles: From preparation to lab-on-a-chip, biosensors, microsystems and microfluidics applications, TrAC, Trends Anal. Chem. 79 (2016) 344-362.

[3] I. Vasconcelos, C. Fernandes, Magnetic solid phase extraction for determination of drugs in biological matrices, TrAC, Trends Anal. Chem. 89 (2017) 41-52.

[4] S. Miltenyi, W. Müller, W. Weichel, A. Radbruch, High gradient magnetic cell separation with MACS, Cytometry A 11 (1990) 231-238.

[5] S.A. Wahajuddin, Superparamagnetic iron oxide nanoparticles: magnetic nanoplatforms as drug carriers, Int. J. Nanomedicine 7 (2012) 3445.

[6] S.R. Dave, X. Gao, Monodisperse magnetic nanoparticles for biodetection, imaging, and drug delivery: a versatile and evolving technology, Wiley Interdiscip. Rev. Nanomed. Nanobiotechnol. 1 (2009) 583-609.

[7] J.M. Perez, T. O'Loughin, F.J. Simeone, R. Weissleder, L. Josephson, DNA-based magnetic nanoparticle assembly acts as a magnetic relaxation nanoswitch allowing screening of DNA-cleaving agents, J. Am. Chem. Soc. 124 (2002) 2856-2857.

[8] J.E. Smith, L. Wang, W. Tan, Bioconjugated silica-coated nanoparticles for bioseparation and bioanalysis, TrAC, Trends Anal. Chem. 25 (2006) 848-855.

[9] N. Kohler, C. Sun, J. Wang, M. Zhang, Methotrexate-modified superparamagnetic nanoparticles and their intracellular uptake into human cancer cells, Langmuir 21 (2005) 8858-8864.

[10] B. Chertok, B.A. Moffat, A.E. David, F. Yu, C. Bergemann, B.D. Ross, V.C. Yang, Iron oxide nanoparticles as a drug delivery vehicle for MRI monitored magnetic targeting of brain tumors, Biomaterials 29 (2008) 487-496.

441 [11] K. Maier-Hauff, F. Ulrich, D. Nestler, H. Niehoff, P. Wust, B. Thiesen, H. Orawa, V. Budach, A. Jordan,
442 Efficacy and safety of intratumoral thermotherapy using magnetic iron-oxide nanoparticles combined with
443 external beam radiotherapy on patients with recurrent glioblastoma multiforme, J. Neuro-Oncol. 103 (2011)
444 317-324.
445 [12] V. Salgueiriño-Maceira, M.A. Correa-Duarte, M. Spasova, L.M. Liz-Marzán, M. Farle, Composite
446 silica spheres with magnetic and luminescent functionalities, Adv. Funct. Mater. 16 (2006) 509-514.
447 [13] G.S. Demirer, A.C. Okur, S. Kizilel, Synthesis and design of biologically inspired biocompatible iron
448 oxide nanoparticles for biomedical applications, J. Mater. Chem. B 3 (2015) 7831-7849.
449 [14] J. Chomoucka, J. Drbohlavova, D. Huska, V. Adam, R. Kizek, J. Hubalek, Magnetic nanoparticles and
450 targeted drug delivering, Pharmacol. Res. 62 (2010) 144-149.
451 [15] A.K. Gupta, M. Gupta, Synthesis and surface engineering of iron oxide nanoparticles for biomedical
452 applications, Biomaterials 26 (2005) 3995-4021.
453 [16] D. Singh, J.M. McMillan, X.-M. Liu, H.M. Vishwasrao, A.V. Kabanov, M. Sokolsky-Papkov, H.E.
454 Gendelman, Formulation design facilitates magnetic nanoparticle delivery to diseased cells and tissues,
455 Nanomedicine 9 (2014) 469-485.
456 [17] W. Wu, Q. He, C. Jiang, Magnetic iron oxide nanoparticles: synthesis and surface functionalization
457 strategies, Nanoscale Res. Lett. 3 (2008) 397.
458 [18] J.R. Stephens, J.S. Beveridge, M.E. Williams, Analytical methods for separating and isolating
459 magnetic nanoparticles, Phys. Chem. Chem. Phys. 14 (2012) 3280-3289.
460 [19] V. Tolmacheva, V. Apyari, E. Kochuk, S. Dmitrienko, Magnetic adsorbents based on iron oxide
461 nanoparticles for the extraction and preconcentration of organic compounds, J. Anal. Chem. 71 (2016) 321-
462 338.
463 [20] Y. Wang, Q. Chen, C. Gan, B. Yan, Y. Han, J. Lin, A review on magnetophoretic immunoseparation,
464 J. Nanosci. Nanotechnol. 16 (2016) 2152-2163.
465 [21] A.A. Hernandez-Hernandez, G.A. Alvarez-Romero, E. Contreras-Lopez, K. Aguilar-Arteaga, A.
466 Castaneda-Ovando, Food Analysis by Microextraction Methods Based on the Use of Magnetic Nanoparticles
467 as Supports: Recent Advances, Food Anal. Methods 10 (2017) 2974-2993.

[22] S. Piovesana, A. L. Capriotti, Magnetic materials for the selective analysis of peptide and protein biomarkers, Curr. Med. Chem. 24 (2017) 438-453.

[23] T. Tangchaikeeree, D. Polpanich, A. Elaissari, K. Jangpatarapongsa, Magnetic particles for in vitro molecular diagnosis: From sample preparation to integration into microsystems, Colloids Surf. B 158 (2017) 1-8.

[24] J.C. Giddings, F. Yang, M.N. Myers, Flow-field-flow fractionation: a versatile new separation method, Science 193 (1976) 1244-1245.

[25] H.B. Rogers, T. Anani, Y.S. Choi, R.J. Beyers, A.E. David, Exploiting size-dependent drag and magnetic forces for size-specific separation of magnetic nanoparticles, Int. J. Mol. Sci. 16 (2015) 20001-20019.

[26] M. Zborowski, L. Sun, L.R. Moore, P.S. Williams, J.J. Chalmers, Continuous cell separation using novel magnetic quadrupole flow sorter, J. Magn. Magn. Mater. 194 (1999) 224-230.

[27] F. Carpino, L.R. Moore, J.J. Chalmers, M. Zborowski, P.S. Williams, Quadrupole magnetic field-flow fractionation for the analysis of magnetic nanoparticles, IOP Publishing. 2005, p. 174.

[28] T. Orita, L.R. Moore, P. Joshi, M. Tomita, T. Horiuchi, M. Zborowski, A quantitative determination of magnetic nanoparticle separation using on-off field operation of quadrupole magnetic field-flow fractionation (QMgFFF), Anal. Sci. 29 (2013) 761-764.

[29] L.R. Moore, P.S. Williams, F. Nehl, K. Abe, J.J. Chalmers, M. Zborowski, Feasibility study of red blood cell debulking by magnetic field-flow fractionation with step-programmed flow, Anal. Bioanal. Chem. 406 (2014) 1661-1670.

[30] L. Pauling, C.D. Coryell, The magnetic properties and structure of hemoglobin, oxyhemoglobin and carbonmonoxyhemoglobin, Proc. Natl Acad. Sci. U.S.A 22 (1936) 210-216.

[31] C.D. Coryell, F. Stitt, L. Pauling, The magnetic properties and structure of ferrihemoglobin (methemoglobin) and some of its compounds, J. Am. Chem. Soc. 59 (1937) 633-642.

[32] E. Wetterskog, A. Castro, L. Zeng, S. Petronis, D. Heinke, E. Olsson, L. Nilsson, N. Gehrke, P. Svedlindh, Size and property bimodality in magnetic nanoparticle dispersions: single domain particles vs. strongly coupled nanoclusters, Nanoscale 9 (2017) 4227-4235.

[33] E. Haladjova, S. Rangelov, M. Geisler, S. Boye, A. Lederer, G. Mountrichas, S. Pispas, Asymmetric Flow Field-Flow Fractionation Investigation of Magnetopolyplexes, Macromol. Chem. Phys. 216 (2015) 1862-1867.

[34] T. Tasci, E. Manangon, D. Fernandez, W. Johnson, B. Gale, Separation of magnetic nanoparticles by cyclical electrical field flow fractionation, IEEE Trans. Magn. 49 (2013) 331-335.

[35] G.R. Ducatte, N.E. Ballou, C. Quang, S.L. Petersen, Separation and characterization of oxide particles by capillary electrophoresis, J. Microcolumn Sep. 8 (1996) 403-412.

[36] C. Quang, S. Petersen, G. Ducatte, N. Ballou, Characterization and separation of inorganic fine particles by capillary electrophoresis with an indifferent electrolyte system, J. Chromatogr. A 732 (1996) 377-384.

[37] S.L. Petersen, N.E. Ballou, Separation of micrometer-size oxide particles by capillary zone electrophoresis, J. Chromatogr. A 834 (1999) 445-452.

[38] N.G. Vanifatova, B.Y. Spivakov, J. Mattusch, U. Franck, R. Wennrich, Investigation of iron oxide nanoparticles by capillary zone electrophoresis, Talanta 66 (2005) 605-610.

[39] M.N. Alves, P.N. Nesterenko, B. Paull, P.R. Haddad, M. Macka, Separation of superparamagnetic magnetite nanoparticles by capillary zone electrophoresis using non-complexing and complexing electrolyte anions and tetramethylammonium as dispersing additive, Electrophoresis (2018).

[40] F. Mérida, A. Chiu-Lam, A.C. Bohórquez, L. Maldonado-Camargo, M.-E. Pérez, L. Pericchi, M. Torres-Lugo, C. Rinaldi, Optimization of synthesis and peptization steps to obtain iron oxide nanoparticles with high energy dissipation rates, J. Magn. Magn. Mater. 394 (2015) 361-371.

[41] D. Baron, P. Dolanská, Z. Medříková, R. Zbořil, J. Petr, On-line stacking of carboxylated magnetite core–shell nanoparticles in capillary electrophoresis, J. Sep. Sci. (2017).

[42] M. Boström, V. Deniz, G. Franks, B. Ninham, Extended DLVO theory: electrostatic and non-electrostatic forces in oxide suspensions, Adv. Colloid Interface Sci. 123 (2006) 5-15.

[43] M. Zborowski, J.J. Chalmers, Magnetophoresis: fundamentals and applications, Wiley Encyclopedia of Electrical and Electronics Engineering (1999) 1-23.

521 [44] G.D. Moeser, K.A. Roach, W.H. Green, T. Alan Hatton, P.E. Laibinis, High-gradient magnetic
522 separation of coated magnetic nanoparticles, AlChE J. 50 (2004) 2835-2848.
523 [45] S. Mirshahghassemi, A.D. Ebner, B. Cai, J.R. Lead, Application of high gradient magnetic separation
524 for oil remediation using polymer-coated magnetic nanoparticles, Sep. Purif. Technol. 179 (2017) 328-334.
525 [46] P.Y. Toh, B.W. Ng, C.H. Chong, A.L. Ahmad, J.-W. Yang, C.J.C. Derek, J. Lim, Magnetophoretic
526 separation of microalgae: the role of nanoparticles and polymer binder in harvesting biofuel, RSC Advances
527 4 (2014) 4114-4121.
528 [47] P.Y. Toh, B.W. Ng, A.L. Ahmad, D.C.J. Chieh, J. Lim, Magnetophoretic separation of Chlorella sp.:
529 role of cationic polymer binder, Process Saf. Environ. 92 (2014) 515-521.
530 [48] J. Lim, S.P. Yeap, C.H. Leow, P.Y. Toh, S.C. Low, Magnetophoresis of iron oxide nanoparticles at low
531 field gradient: the role of shape anisotropy, J. Colloid Interface Sci. 421 (2014) 170-177.
532 [49] P. Zhang, S. Park, S.H. Kang, Size-dependent magnetophoresis of native single super-paramagnetic
533 nanoparticles in a microchip, Chem. Commun. 49 (2013) 7298-7300.
534 [50] R. Zhou, C. Wang, Microfluidic separation of magnetic particles with soft magnetic microstructures,
535 Microfluid. Nanofluidics 20 (2016) 48.
536 [51] V. Kumar, P. Rezai, Multiplex Inertio-Magnetic Fractionation (MIMF) of magnetic and non-
537 magnetic microparticles in a microfluidic device, Microfluid. Nanofluidics 21 (2017) 83.
538 [52] S. Dutz, M. Hayden, U. Häfeli, Fractionation of magnetic microspheres in a microfluidic spiral:
539 Interplay between magnetic and hydrodynamic forces, PLoS One 12 (2017) e0169919.
540 [53] V. Cardoso, D. Miranda, G. Botelho, G. Minas, S. Lanceros-Méndez, Highly effective clean-up of
541 magnetic nanoparticles using microfluidic technology, Sens. Actuators B Chem. 255 (2018) 2384-2391.
542 [54] R. Zhou, F. Bai, C. Wang, Magnetic separation of microparticles by shape, Lab Chip 17 (2017) 401-
543 406.

544

545 Table 1 – Particle composition and size, magnetic field applied, separation principle, separation time and complexity of the infrastructure used for M(N)Ps and

546 magnetically susceptible RBCs between 2013 and 2018.

Particle composition	**Particle size (nm)**	**Magnetic field applied**	**Separation principle**	**Separation time**	**Complexity of the infrastructure**	**Ref**
Starch-coated magnetite (nano)particles	50–400	51 mm length Grade N42 diametrically magnetized NdFeB cylinder	MFFF	<1 hour	Basic laboratory equipment	[25]
Dextran-coated magnetite nano(particles)	90 and 200	Quadrupole electromagnet	MQFFF	50 min	Stainless-steel cylinder within a quadrupole electromagnet implemented into a flow injection setup with downstream optical detection	[28]
RBCs	8000	Quadrupole magnet	MQFFF	25 min	Cylindrical flow channel centred inside of a quadrupole magnet with downstream light scattering detection	[29]
Carboxydextran-coated maghemite nanoparticles	6 – 60	n.a.	AF4	15 min	AF4 instrument connected to MALLS detection	[32]
Hybrid polymer magnetic micelles	54	n.a.	AF4	15 min	AF4 instrument connected to UV and MALLS detection	[33]
Lipid and polystyrene sulfonate-coated magnetite nanoparticles	50 and 100	n.a.	CyEFFF	30 min	HPLC pump connected to an EFFF channel with downstream UV detection; ac and dc voltages induced by a signal generator and a dc power supply	[34]
Polyvinylpyrrolidone (PVP)-coated magnetic particles	127	0.56 T permanent magnetic assembly consisting of two 2x 4 x 0.5 inch	HGMS	1 hour	HGMS instrument	[45]

		NdFeB blocks with a minimum gap of 5/8 inch				
Poly (diallyl dimethylammonium chloride) (PDDA) and chitosan (Chi)-coated magnetic nanoparticles	50	NdFeB permanent magnet	LGMS	6 min	Basic laboratory equipment	[46]
Poly(diallyldimethylamonium chloride) (PDDA)-coated iron oxide nanoparticles	50 nm (spherical) and 20 x 300 nm (rod-like)	Cylindrical shaped N50-graded NdBFe (1.20 T) and Alnico permanent magnet (1.45 T) with 14 mm in diameter and 15 mm in length	LGMS	6 hours	Basic laboratory equipment	[48]
Bare and carboxylated iron oxide nanoparticles	7 - 13 (bare iron oxide nanoparticles) and 10 (carboxylated iron oxide nanoparticles)	n.a.	CE	12 min	CE instrument	[39]
Carboxylated iron oxide nanoparticles	75	n.a.	CE	5 min	CE instrument	[41]
Polydisperse magnetic particles	150 and 500	Permanent NbFeB magnet (6 mm length, 4 mm width, and 3 mm thickness)	Microchip magnetophoresis	15 sec	Microchip fabricated in PDMS with a side permanent magnet, a Gaussmeter, and DIC detection	[49]
Iron oxide magnetic beads	5000	Soft magnetic microstructures made of a mixture of iron powder and PDMS into a	Microchip magnetophoresis	<2 sec	Microchip fabricated in PDMS mounted in an inverted microscope connected to a high-speed camera, placed in the centre of parallel permanent magnets	[50]

		prefabricated channel				
Polystyrene (5000 and 11000 nm) and polyethylene (35000 nm) magnetic beads	5000, 11000, and 35000	Permanent NbFeB N42 grade cuboid magnet	Microchip magnetophoresis	15 min	Microchip fabricated in PDMS with a side permanent magnet mounted in an inverted microscope connected to a high-speed camera	[51]
Microspheres composed of styrene-maleic acid copolymer matrix encapsulating 50% by mass magnetite cores	2000, 6000 and 12000	Octupolar array of permanent magnets	Microchip magnetophoresis	10 sec	Microchip fabricated in PDMS with a spiral channel centred with respect to the octupolar magnetic array	[52]
Magnetite nanoparticles	10	Permanent NbFeB magnet	Microchip magnetophoresis	>1 hour	Microchip fabricated in PDMS with permanent magnet mounted in an inverted microscope connected to a high-speed camera	[53]
Magnetite-doped and uncross-linked polystyrene particles with spherical and elliptical shapes	7000	Halbach array	Microchip magnetophoresis	<2 sec	Microchip fabricated in PDMS placed in the center of the Halbach array mounted in an inverted microscope connected to a high-speed camera	[54]

AF4: Asymmetrical field flow fractionation; **CE:** Capillary electrophoresis; **CyEFFF:** Cyclical electrical field flow fractionation; **HGMS:** High gradient magnetic separation; **LGMS:** Low gradient magnetic separation; **MALLS:** Multi-angle laser light scattering; **MFFF:** Magnetic field flow fractionation; **MQFFF:** Magnetic quadrupole field flow fractionation; **RBCs:** Red blood cells.